applied sciences

MDPI

Article

Researching the Properties of Samples Fabricated Using Selective Laser Melting from A High-Temperature Nickel-Based Alloy

Alexey Mazalov [1], Dmitry Shmatov [2], Lydia Zelenina [1], Dmitry Platko [1], Vladimir Promakhov [3], Alexander Vorozhtsov [3] and Nikita Schulz [3,*]

[1] JSC Center of Technological Competence of Additive Technologies, 396658 Voronezh, Russia; aleksey.mazalov@vselmash.ru (A.M.); lidiya.zelenina@vselmash.ru (L.Z.); dmitry.platko@3d-made.com (D.P.)
[2] Faculty of Mechanical Engineering and Aerospace Engineering, Voronezh State Technical University, Moscow Avenue, 14, 394026 Voronezh, Russia; rd-vgtu@mail.ru
[3] Scientific and Educational Center "Additive technologies", National Research Tomsk State University, Lenin Avenue, 36, 634050 Tomsk, Russia; vvpromakhov@mail.ru (V.P.); abv1953@mail.ru (A.V.)
* Correspondence: schulznikita97@gmail.com; Tel.: +7-961-890-95-03

Abstract: A possible application of a metal powder composition made of a high-temperature nickel-based alloy with high heat strength (the material is analogous to Inconel 718) in selective laser melting (SLM, an additive manufacturing technology) was considered. Peculiarities of material formation in the course of selective laser melting of the metal have been researched, and the mechanical properties of the material were determined. The effect of the thermal treatment mode on the mechanical characteristics was investigated. It was shown that the tensile strength of samples made of a high-temperature nickel alloy when the samples have not been subjected to thermal treatment is ~950 MPa; samples subjected to thermal treatment is ~1070 MPa.

Keywords: additive manufacturing technologies; selective laser melting; metal powder composition; high heath strength; nickel alloy; mechanical properties; tensile strength; hardness

Citation: Mazalov, A.; Shmatov, D.; Zelenina, L.; Platko, D.; Promakhov, V.; Vorozhtsov, A.; Schulz, N. Researching the Properties of Samples Fabricated Using Selective Laser Melting from A High-Temperature Nickel-Based Alloy. *Appl. Sci.* **2021**, *11*, 1419. https://doi.org/10.3390/app11041419

Academic Editor: Alireza Kashani
Received: 11 January 2021
Accepted: 1 February 2021
Published: 4 February 2021

1. Introduction

Aerospace parts are subjected to high mechanical and thermal loads throughout their entire operational lives. Therefore, certified parts must have high density, low surface roughness, and a low level of residual stress, as well as high tensile strength and fatigue strength. In addition, to achieve the desired aerodynamic flows and low fuel consumption, complex geometric shapes and light weight are required [1]. A gas turbine blade is a great example of complex geometry with internal cooling ducts fabricated for maximum possible energy while ensuring proper cooling during operation. However, the fabrication of such geometric shapes and cooling ducts is limited by traditional technologies that prevent us from researching a wider range of designs with new functional capabilities [2,3].

Thanks to good oxidation resistance and fatigue strength, high-temperature Ni-based alloys are widely used in rocket engineering and other industries where heat strength and heat resistance are critical requirements [4,5]. However, the Inconel 718 (IN718) alloy, for example, is a hardly machinable material due to its inability to quench. IN718 has low heat conductivity, which causes a sharp temperature gradient at the tool-shavings boundary, which leads to increased tool wear [2]. Therefore, a more suitable technology should be researched for fabricating parts from IN718.

Additive manufacturing (AM) technologies, specifically selecting laser melting, offer a flexible solution to the above problems [6,7]. Selective laser melting (SLM) provides freedom for design necessary for manufacturing parts with complex geometry without using ad-hoc tools, which allows for saving time and materials. The main purpose of SLM is the fabrication of quality parts with predictable mechanical properties, such as density,

surface roughness, residual stress, tensile strength, etc. The main process parameters of SLM are the laser power, laser scanning speed, hatch spacing, and scanning strategy, all of which thus create certain microstructures and properties for the fabricated part.

Despite some advantages, the SLM process has some drawbacks: microstructure inhomogeneity and randomly scattered defects, which lead to the deterioration of mechanical properties [8,9]. For example, in the course of SLM of IN718, anisotropy, microstructure inhomogeneity, residual stress, undesired phases, and incomplete fusion defects are normally caused by the fast crystallization of molten metal. These factors have complex effects on the mechanical properties of materials, especially compared to their forged and cast counterparts [10]. To optimize mechanical properties, thermal treatment is subsequently used to modify the structure of grains [11,12], as well as their type, shape, and size as fabricated from IN718 [13,14]. Therefore, we need to research the correlation between the creeping flow properties and microstructural defects created during AM and thermal treatment. Thus, this work is devoted to the maturing of 3D printing modes for parts fabricated from a high-temperature nickel-based alloy, the research of the mechanical properties of experimental samples, and the comparison of thermal treatment modes.

2. Materials and Methods

A nickel-based high-temperature alloy with high heat strength was selected for research.

The chemical composition of the powder composition used is provided in Table 1. The powder does not contain impurities.

Table 1. The chemical composition of the researched materials (mixture of the powders, which was alloyed during the selective laser melting (SLM)) and the IN718 alloy.

Material Grade	Elements Mass Ratio, %						
The powder composition used	C 0.05 Mo 2.9	S 0.0046 Nb 4.8	P 0.015 Al 0.47	Si 0.45 Ti 1.1	Mn 0.3 Cu 0.05	Cr 18.5 Co 0.1	Ni 51.3 Fe remaining
Inconel 718	C ≤0.08 Mo 2.8 ÷ 3.3	S ≤0.015 Nb 4.75 ÷ 5.5	P ≤0.015 Al 0.2 ÷ 0.8	Si ≤0.35 Ti 0.65 ÷ 1.15	Mn ≤0.35 Cu ≤0.3	Cr 17 ÷ 21 Co ≤1.0	Ni 50 ÷ 55 Fe remaining

SEM images of the metal powder composition are shown in Figure 1. Particle sizes are 20–45 μm, and their shape is almost spherical. The pour density of 4.39 g/cm^3 and the fluidity of 13.6 confirm good flowability that is necessary for the quality distribution of the material in the equipment.

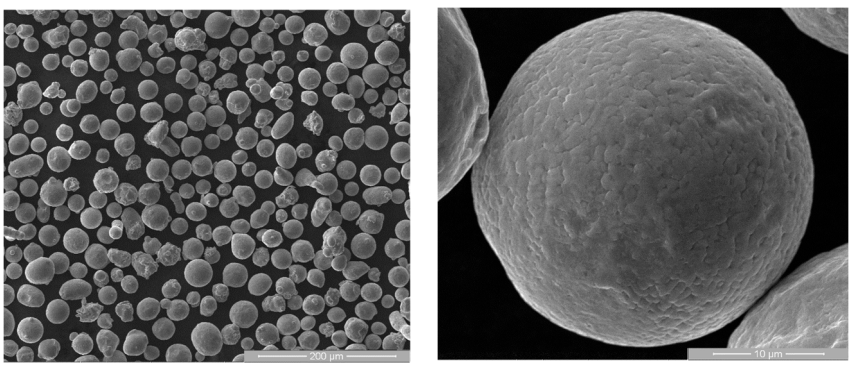

Figure 1. SEM images of the powder metal composition (mixture of the powders).

In this article, an SLM 280HL machine (maximum laser power of 400 W, build chamber—280 × 280 × 350 mm, IPG Laser—laser beam manufacturer, laser beam

wavelength—1070 nm) was used for the 3D printing of the samples; the machine utilizes selective laser melting. High-purity argon was used as the process gas (the volume fraction of argon is not less than 99.998%).

The SEM images were taken using QUANTA 200 3D (accelerating voltage: 200–30,000 V), a dual-beam scanning electron microscope (SEM), and a focused ion beam (FIB) instrument. The equipment used for mechanical testing is as follows: a dual-column floor-mounted 5980 frame (Instron 5982, force 15 kN), a standard compression testing device, a standard extension testing device (clamping jaws), an SHCC-1-150-0.01 caliper, an MK-10 drop hammer rig: maximum drop hammer test impact energy—98.1 J (10 kgs·m), drop hammer speed at impact—5 m/s and an MPP-2 microscope.

The shape and size of the fabricated tensile test specimens are shown in Figure 2.

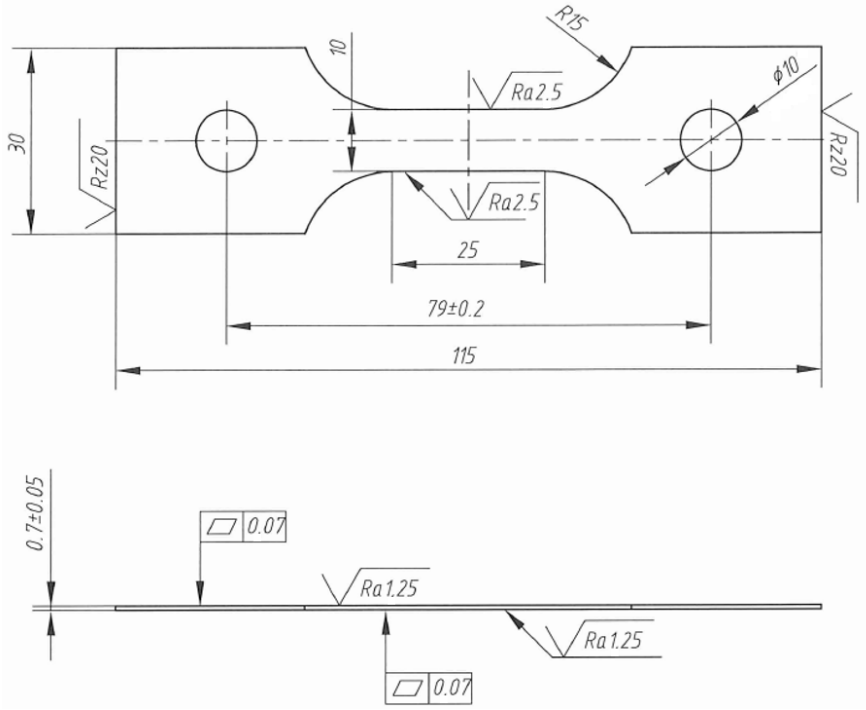

Figure 2. Configuration of tensile test pieces used in this study.

The first research phase was the selection of the optimal metal powder composition melting mode.

The most significant factors in this experiment were laser radiation power and laser scanning speed that were changed during the build process at a certain interval.

The recorded factors:

- distance between tracks—140 μm;
- layer thickness—30 μm;
- inert medium—argon;
- fractional composition—20–45 μm;
- laser beam diameter—0.074 mm;
- path overlap—20 μm;
- scanning speed—900 mm/c;
- X and Y offset—1 mm.

The main experiment parameters, laser power (P, in Watts) and laser scanning speed (υ, in mm/s), the scan direction is the *x*-axis, were determined from the analysis of the literature [15–21]. Based on the selected value range for P and υ (P ranged from 170 to 270 W, υ ranged from 750 to 1150 mm/s), a matrix of cube-shaped samples was built (with the size of 7 × 7 × 5 mm) for further metallographic studies for finding pores on the surface.

3. Results

The proportion of pores for most parameter combinations was between 0.1 and 2.5%. The relative densities of all samples were measured by processing optical photographs of the sample surface using the Image-Pro Plus software. We made cross-sections on the XY side.

The pore percent ratio was calculated via the formula

$$P = \frac{S_H}{S_{SA}}; 100\% \quad (1)$$

where P is porosity, %;

SH—area occupied by the pores on the sample's surface, μm^2;
SSA—area of the sample's surface, μm^2.

It was visible in this range that as the speed increased, the ratio of pores grew up to its maximum value, depending on the power of the laser used. The most noticeable combinations were the combination of the lowest energy parameters and highest speeds (170 W and 1150 mm/s). At such low input energy, the pore ratio was 2.5%. These observations become clearer if we build a porosity histogram from the values of the researched parameters (Figure 3).

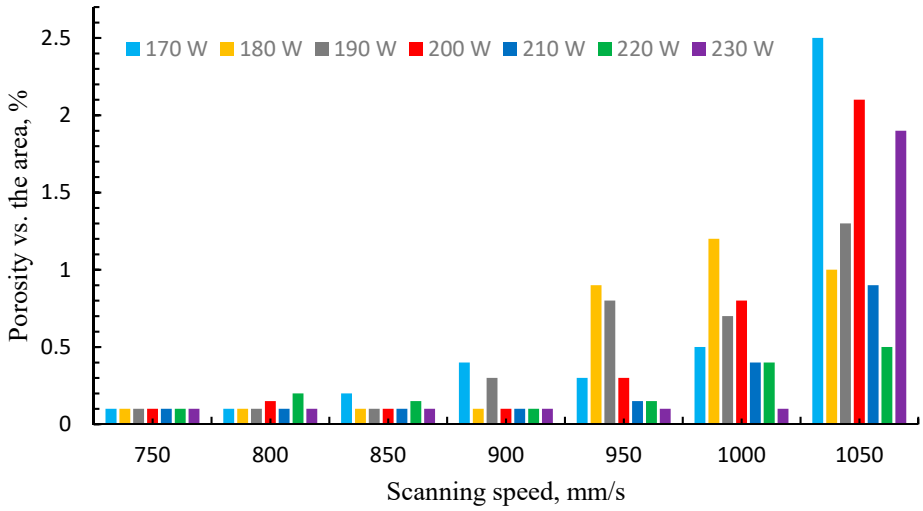

Figure 3. A histogram of porosity values depending on laser power and scanning speed.

The results of metallographic studies are provided in Figures 4 and 5. It was shown that pores with the size of over 40 µm were present on the surface of experimental sample 230 W, 1050 mm/s.

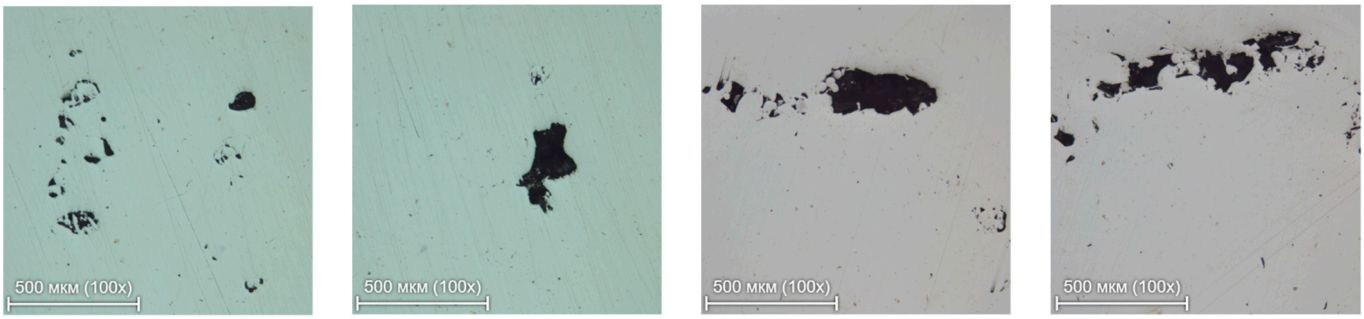

(**a**) (**b**)

Figure 4. Photographs of the sample 230 W, 1050 mm/s: (**a**) the topmost surface taken from different areas; (**b**) lateral surface taken from different areas.

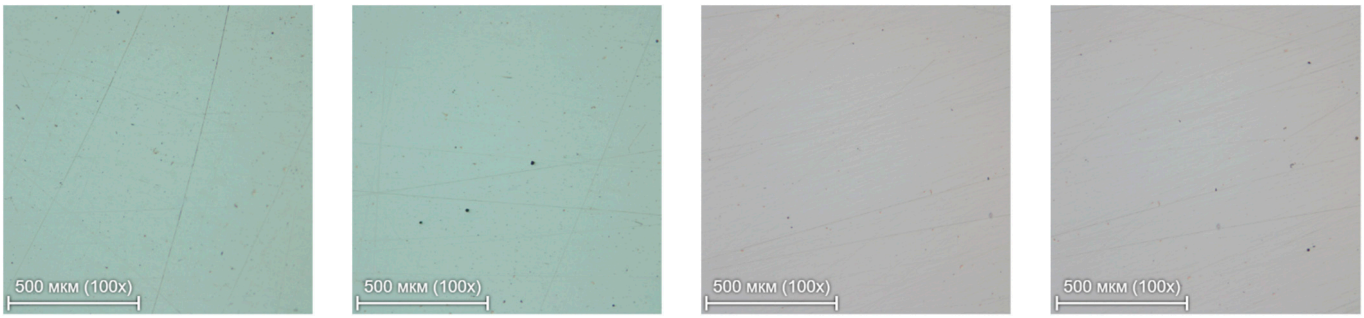

(**a**) (**b**)

Figure 5. Photographs of the sample 200 W, 900 mm/s: (**a**) the topmost surface taken from different areas; (**b**) lateral surface taken from different areas.

For the purpose of this research, the authors kept to the following technical specifications:

- Defects (micropores) not exceeding 40 μm were allowed [15].
- The relative density of the material must be at least 99.4%.

Based on the above, an optimal melting mode for the metal powder composition was found; this mode was used for the 3D printing of the samples for mechanical tests (laser power of 190 ± 20 W and laser scanning speed of 855 ± 90 mm/s).

The samples were oriented vertically on the build platform. The mechanical tests were performed on the samples not subjected to thermal treatment and on the samples subjected to two types of thermal treatment. One of the treatment types was homogenization with subsequent double aging, which is a standard mode widely used for deformed or cast IN718 alloy [22]: 1065 °C × 1.5 h/air cooled, 760 °C × 10 h/cooled in a furnace to 650 °C (at the speed of 55 °C/h) and then kept at room temperature for over 8 h. The other treatment type was homogenization with single aging: homogenization at 1150 °C over 2 h (air-cooled), aging at 700 °C over 12 h followed by water cooling [23].

The results of the mechanical tests are provided in Table 2 and Figures 6 and 7. The hardness measurement was prepared on the surface of the sample along the Z-axis.

Table 2. The mechanical testing results of the fabricated samples.

No.	Thermal Treatment Type	Yield Strength MPa	Travel mm	Extension Deformation %	Hardness Hv GPa
1	No TT	949.5	6.0	20.4	3.5
2		944.5	5.9	19.8	3.5
3		928.8	3.2	20.7	3.4
4		988.1	3.9	19.4	3.9
5	First TT type	1278.6	2.5	9.4	5.1
6		1231.9	2.4	9.0	4.9
7		1126.3	2.1	7.9	5.0
8		1191.7	2.2	8.5	4.9
9		1167.9	2.6	9.7	5.1
10	Second TT type	1104.7	2.2	7.9	4.9
11		1033.1	2.0	7.2	5.0
12		1100.5	2.3	8.2	4.7
13		1069.8	2.4	8.4	4.9
14		1117.8	2.5	8.7	4.6

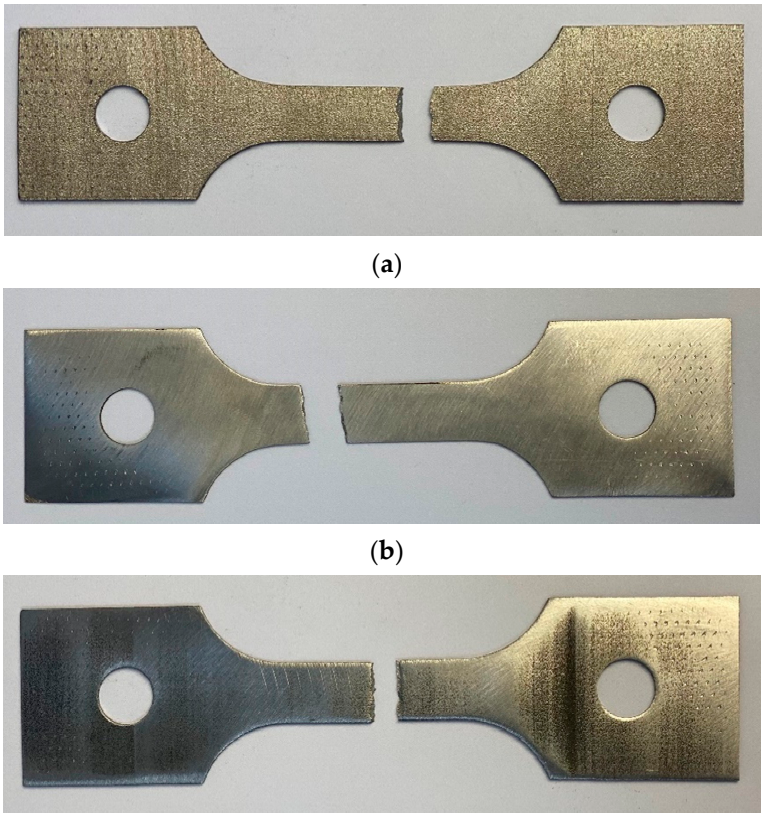

(**a**)

(**b**)

(**c**)

Figure 6. Photographs of the samples after the test. (**a**)—sample without thermal treatment; (**b**)—sample after type 1 thermal treatment; (**c**)—sample after type 2 thermal treatment.

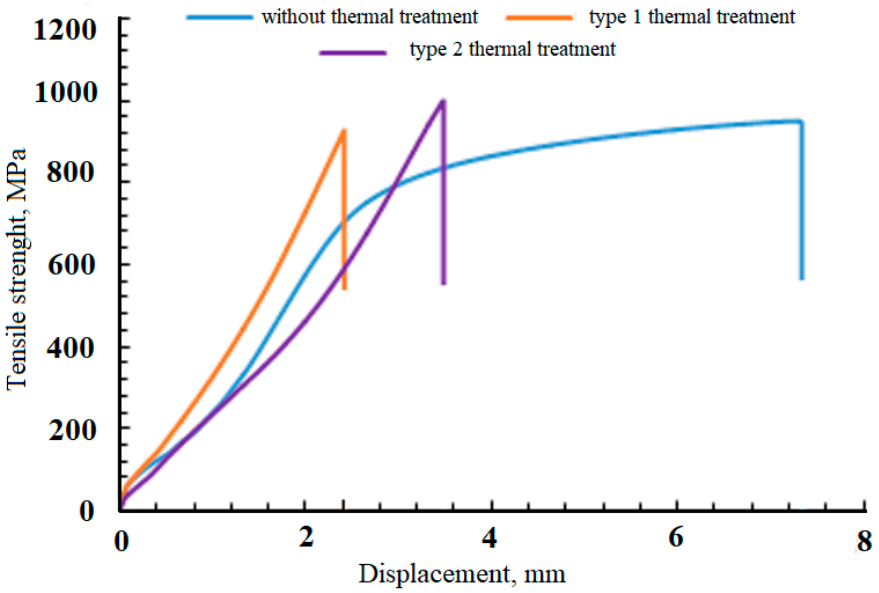

Figure 7. A graph of the dependency of the mechanical strength on the travel distance.

The first and the second types of thermal treatment increased the ultimate strength by ~21% and 12%, respectively. Meanwhile, thermal treatment reduced tensile deformation by over two times. We must note that after the TT, the samples' hardness increased by ~25% and 28%, respectively. However, the values of the mechanical properties of the samples after two thermal treatment types did not differ significantly.

Figure 8 shows the morphology of the destruction of samples after extension tests. The samples subjected and not subjected to thermal treatment had differing microstructures. The fractures found in the areas of the material not subjected to thermal treatment featured dimples, gradual ridges, sharp edges, and flat ridges whose dimensions ranged from 100 to 200 μm. In the area, many large dimples with a diameter of over 120 μm were present.

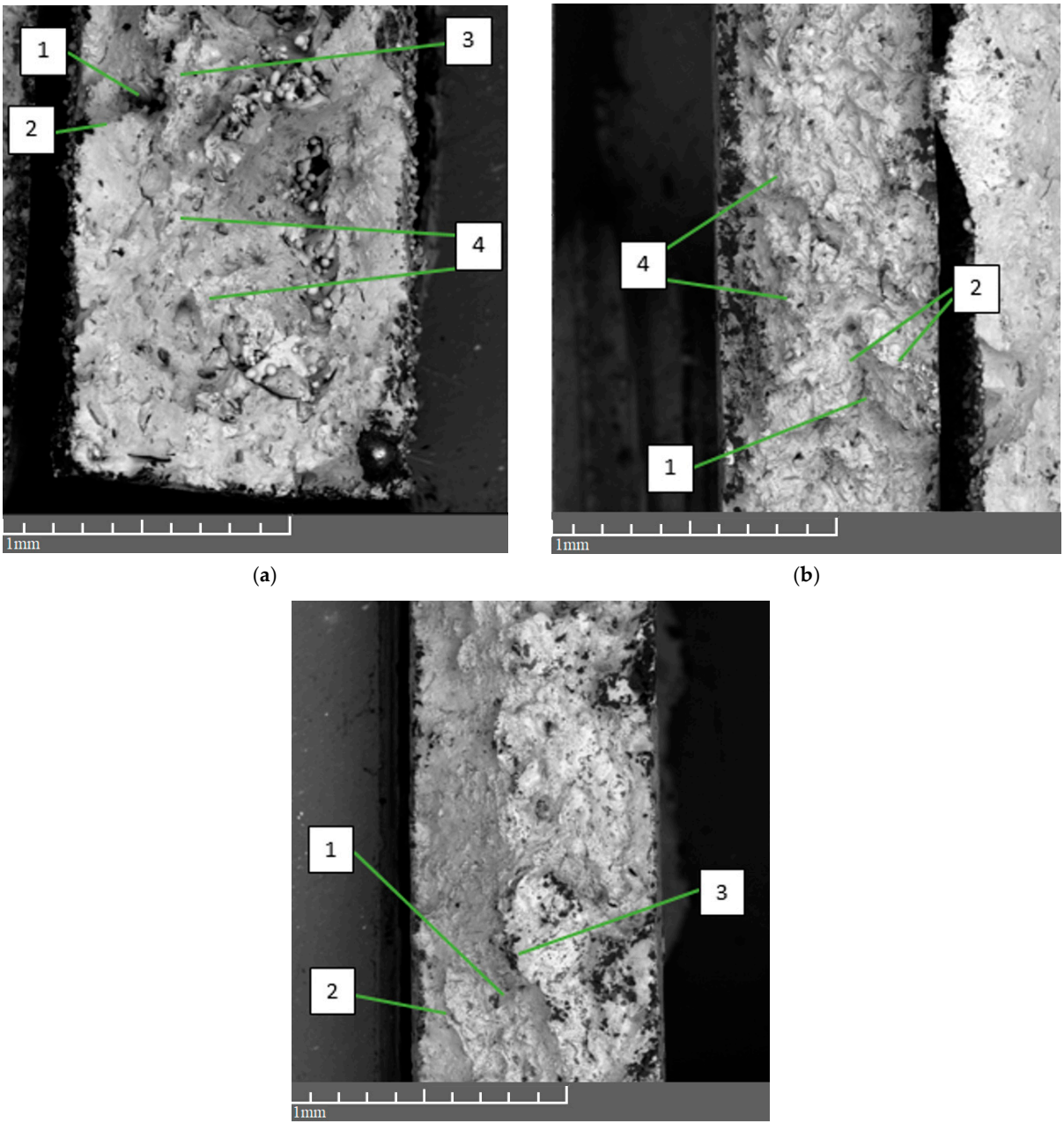

Figure 8. SEM images of the experimental samples: (**a**)—sample without thermal treatment; (**b**)—sample after type 1 thermal treatment type; (**c**)—sample after type 2 thermal treatment) (1—dimples, 2—sharp edges, 3—flat ridges, 4—gradual ridges).

Furthermore, after different treatment types, dimples, gradual ridges, sharp edges, and flat ridges were found on the material surface, and the dimensions of those ranged between 80 and 160 μm, so they were somewhat smaller as compared to the untreated material. It was supposed that defects, unmelted particles, and pores may cause crack propagation at interface boundaries.

4. Discussion

The presented thermal treatment modes were selected based on the analysis of the literature in terms of the effect of thermal treatment on the mechanical properties of metals manufactured by AM [22–29]. The authors of [26] found that the creeping flow properties of IN718 samples alongside the 3D printing direction were better compared to those alongside the scanning direction. Such characteristics of anisotropic creeping flow are mainly explained by the difference in the Jung modulus directions and differing number of grain boundaries. The authors of [27] supposed that the location of the inter-dendrite phase (such as the δ phase in the IN718 alloy) may reduce the creeping flow duration and plasticity of the samples. According to [25], thermal treatment at high temperatures may lead to re-crystallization and a high percent of dual boundaries in the C263 superalloy fabricated by selective laser melting, which hinders the growth of creeping flow cracks. As for the IN718 alloy, thermal treatment not only adjusted the grain size but also caused different precipitation states. After aging, the properties of IN718 treated at a temperature slightly above 1000 °C were better than those of the material treated at a lower temperature. This is explained by the further dissolution of the Laves phase or δ, and thus, more γ′ and γ″ hardening precipitations form in the course of subsequent aging [28,29].

The 3D-printed sample not subjected to TT demonstrated the lowest tensile strength (952.7 MPa) and the highest plastic deformation (20%) among the investigated samples. Increased tensile strength (1055.2 MPa) and reduced elongation (9%) were caused by type 1 thermal treatment. After type 2 thermal treatment, tensile strength was 1069.8 MPa, and extension deformation was at 8%, which is in agreement with the data recorded by other researchers [30–32].

Figure 6 and Table 2 show that at room temperature, the tensile strength, ultimate strength, and relative elongation of the tested material fabricated by SLM were higher than those of cast Inconel 718 alloy [33]. On the one hand, since the SLM process was characterized by a very high cooling rate, the printed part had a finer microstructure compared to the cast part. On the other hand, in the prominent Laves phase, casting shrinkage and dispersed shrinkage caused by the macro segregation of the components often occur in cast items, so the respective amount of hardening precipitations was reduced as well. Therefore, the investigated material fabricated by SLM was better when a fine Laves phase was precipitated in intercrystalline regions. However, as compared to forged Inconel 718, hardening particles of the second phase precipitate in lesser quantities in the researched selective material melted by laser, while the amount of a brittle Laves phase increased [33].

5. Conclusions

1. It was shown that the shape of the particles of the metal powder composition was spherical, and the fractional composition was 20–45 μm. It was established that the material used was analogous to the Inconel 718 alloy in terms of its chemical composition.

2. In the course of the conducted experiments, an efficient melting mode for the high-temperature nickel-based metal powder composition was determined: laser power 190 ± 20 W and laser scanning speed 855 ± 90 mm/s.

3. The changes in the mechanical properties of the alloy were investigated, specifically, the tensile strength of samples made of high-temperature nickel alloy where the samples were not subjected to thermal treatment was 952 MPa; for samples subjected to type 1 thermal treatment, it was 1055 MPa; for samples subjected to type 2 thermal treatment, it was 1070 MPa.

Thus, it can be concluded that the matured technology of selective laser melting provides for an advanced set of mechanical properties is promising for further fabrication of parts of high-temperature nickel alloys.

Author Contributions: Conceptualization, A.M. and V.P.; methodology, D.S., L.Z., and D.P.; validation, A.V., N.S.; resources, A.M. and V.P.; writing—original draft preparation, A.M., V.P., D.S., and N.S.; writing—review and editing, D.P. and; visualization, A.V.; supervision, A.M. and V.P. All authors have read and agreed to the published version of the manuscript.

Funding: The research receiving materials has been conducted with the financial support of the Ministry of Science and Higher Education of the Russian Federation for the purpose of the Federal Targeted Program (Agreement No. 05.607.21.0313, project ID—RFMEFI60719X0313). Work on the study of the structure and properties of materials was performed at the expense of the Russian Science Foundation (project 20-79-10086).

Institutional Review Board Statement: Not applicable.

Informed Consent Statement: Not applicable.

Conflicts of Interest: The authors declare no conflict of interest.

References

1. Caiazzo, F.; Alfieri, V.; Corrado, G.; Argenio, P. Laser powder-bed fusion of Inconel 718 to manufacture turbine blades. *Int. J. Adv. Manuf. Technol.* **2017**, *93*, 4023–4031. [CrossRef]
2. Balbaa, M.; Mekhiel, S.; Elbestwai, M.; Mclsaac, J. On selective laser melting of Inconel 718: Densification, surface roughness, and residual stresses. *Mater. Des.* **2020**, *193*, 108818. [CrossRef]
3. Lu, Z.; Cao, J.; Jing, H.; Liu, T.; Lu, F.; Wang, D.; Li, D. Review of main manufacturing processes of complex hollow turbine blades: This paper critically reviews conventional and advanced technologies used for manufacturing hollow turbine blades. *Virtual Phys. Prototyp.* **2013**, *8*, 87–95. [CrossRef]
4. Brandl, E.; Heckenberger, U.; Holzinger, V.; Buchbinder, D. Additive manufactured AlSi10Mg samples using Selective Laser Melting (SLM): Microstructure, high cycle fatigue, and fracture behavior. *Mater. Des.* **2017**, *34*, 159–169. [CrossRef]
5. Yadollahi, A.; Shamsaei, N. Additive manufacturing of fatigue resistant materials: Challenges and opportunities. *Int. J. Fatigue* **2017**, *98*, 14–31. [CrossRef]
6. DebRoy, T.; Wei, H.; Zuback, J.; Mukherjee, T.; Elmer, J.; Milewski, J.; Beese, A.; Wilson-Heid, A.; De, A.; Zhang, W. Additive manufacturing of metallic components–process, structure and properties. *Prog. Mater. Sci.* **2018**, *92*, 112–124. [CrossRef]
7. Wang, X.; Gong, X.; Chou, K. Review on powder-bed laser additive manufacturing of Inconel 718 parts. *Proc. Inst. Mech. Eng. B J. Eng. Manuf.* **2017**, *231*, 1890–1903. [CrossRef]
8. Rowcliffe, A.F.; Mansur, L.K.; Hoelzer, D.; Nanstad, R. Perspectives on radiation effects in nickel-base alloys for applications in advanced reactors. *J. Nucl. Mater.* **2009**, *392*, 341–352. [CrossRef]
9. Pollock, T.M.; Tin, S. Nickel-based superalloys for advanced turbine engines: Chemistry, microstructure, and properties. *J. Propuls. Power* **2006**, *22*, 361–374. [CrossRef]
10. Wang, L.Y.; Zhou, Z.J.; Li, C.P.; Chen, G.F.; Zhang, G.P. Comparative investigation of small punch creep resistance of Inconel 718 fabricated by selective laser melting. *Mater. Sci. Eng. A* **2019**, *745*, 31–38. [CrossRef]
11. Kuo, Y.L.; Nagahari, T.; Kakehi, K. The effect of post-processes on the microstructure and creep properties of alloy718 built up by selective lasermelting. *Materials* **2018**, *116*, 996. [CrossRef] [PubMed]
12. Wang, Y.; Yu, E.; Yang, H.; Zhang, Q. Growth behavior of Li & Sb doped alkalis niobate synthesized by hydrothermal method. *Mater. Design* **2016**, *110*, 51–59.
13. Gallmeyer, T.G.; Moorthy, S.; Kappes, B.; Mills, M.; Amin-Ahmadi, B.; Stebner, A. Knowledge of process-structure-property relationships to engineer better heat treatments for laser powder bed fusion additive manufactured Inconel 718. *Addit. Manuf.* **2020**, *31*, 100977. [CrossRef]
14. Shassere, B.; Greeley, D.; Okello, A.; Kirka, M.; Nandwana, P.; Denoff, R. Correlation of microstructure to creep response of hot isostatically pressed and aged electron beam melted Inconel 718. *Metall. Mater. Trans. A* **2018**, *49*, 5107–5117. [CrossRef]
15. Zhang, B.; Liao, H.; Coddet, C. Effects of processing parameters on properties of selective laser melting Mg-9%Al powder mixture. *Mater. Des.* **2012**, *34*, 753–758. [CrossRef]
16. Kablov, E.N.; Evgenov, A.G.; Ospennikova, O.; Semenov, B.; Semenov, A.; Korolev, V. Metal Power Compositions for the EP648 Heat Resistant Alloy Manufactured by All-Russian Research Institute for Aircraft Materials VIAM for Selective Laser Melting, Laser Metal Deposition and Metal Injection Molding Technologies. *BMSTU J. Mech. Eng.* **2016**, *9*. [CrossRef]
17. Zhang, B.; Li, Y.; Bai, Q. Defect Formation Mechanisms in Selective Laser Melting: A Review. *Chin. J. Mech. Eng.* **2017**, *30*, 515–527. [CrossRef]
18. Zhang, P.; He, N.; Liu, F.; Zhang, K.; Jiang, J.; Zhang, D. Evaluation of Low Cycle Fatigue Performance of Selective Laser Melted Titanium Alloy Ti–6Al–4V. *Metals* **2019**, *9*, 1041. [CrossRef]
19. Sotov, A.V.; Agapovichev, A.V.; Smelov, V.; Kyarimov, R. Development Algorithm of the Technological Process of Manufacturing Gas Turbine Parts by Selective Laser Melting. *IOP Conf. Ser. Mater. Sci. Eng.* **2018**, *302*, 012065. [CrossRef]
20. Mendagaliev, R.; Klimova-Korsmik, O.; Promakhov, V.; Schulz, N.; Zhukov, A.; Klimenko, V.; Olisov, A. Heat Treatment of Corrosion Resistant Steel for Water Propellers Fabricated by Direct Laser Deposition. *Materials* **2020**, *13*, 2738. [CrossRef]

21. Promakhov, V.; Zhukov, A.; Ziatdinov, M.; Zhukov, I.; Schulz, N.; Kovalchuk, S.; Dubkova, Y.; Korsmik, R.; Klimova-Korsmik, O.; Turichin, G.; et al. Inconel 625/TiB_2 Metal Matrix Composites by Direct Laser Deposition. *Metals* **2019**, *9*, 141. [CrossRef]
22. Popovich, V.A.; Borisov, E.V.; Popovich, A.; Sufiiarov, V.; Masaylo, D.; Alzina, L. Impact of heat treatment on mechanical behaviour of Inconel 718 processed with tailored microstructure by selective laser melting. *Mater. Des.* **2017**, *131*, 12–22. [CrossRef]
23. Li, X.; Shi, J.; Cao, G.; Russell, A.; Zhou, Z.; Li, C.; Chen, G. Improved plasticity of Inconel 718 superalloy fabricated by selective laser melting through a novel heat treatment process. *Mater. Des.* **2019**, *180*, 107915. [CrossRef]
24. Hilal, H.; Lancaster, R.; Jeffs, S.; Boswll, J.; Stapleton, D.; Baxter, G. The influence of process parameters and build orientation on the creep behaviour of a laser powder bed fused Ni-based superalloy for aerospace applications. *Materials* **2019**, *12*, 1390. [CrossRef] [PubMed]
25. Davies, S.J.; Jeffs, S.P.; Coleman, M.; Lancaster, R. Effects of heat treatment on microstructure and creep properties of a laser powder bed fused nickel superalloy. *Mater. Des.* **2018**, *159*, 39–46. [CrossRef]
26. Kunze, K.; Etter, T.; Grässlin, J.; Shklover, V. Texture, anisotropy in microstructure and mechanical properties of IN738LC alloy processed by selective laser melting (SLM). *Mater. Sci. Eng. A* **2015**, *620*, 213–222. [CrossRef]
27. Kuo, Y.; Horikawa, S.; Kakehi, K. Effects of build direction and heat treatment on creep properties of Ni-base superalloy built up by additive manufacturing. *Scr. Mater.* **2017**, *129*, 74–78. [CrossRef]
28. Pröbstle, M.; Neumeier, S.; Hopfenmüller, J.; Freund, L.; Niendorf, T.; Schwarze, D.; Göken, M. Superior creep strength of a nickel-based superalloy produced by selective laser melting. *Mater. Sci. Eng. A* **2016**, *674*, 299–307. [CrossRef]
29. Brenne, F.; Taube, A.; Probste, M.; Neumeir, S.; Schwarze, D.; Schaper, M.; Niendorf, T. Microstructural design of Ni-base alloys for high-temperature applications: Impact of heat treatment on microstructure and mechanical properties after selective laser melting. *Prog. Addit. Manuf.* **2016**, *1*, 141–151. [CrossRef]
30. Trosch, T.; Strößner, J.; Völkl, R.; Glatzel, U. Microstructure and mechanical properties of selective laser melted Inconel 718 compared to forging and casting. *Mater. Lett.* **2016**, *164*, 428–431. [CrossRef]
31. Raghavan, S.; Zhang, B.; Wang, P.; Sun, C.; Nai, M.; Li, T.; Wei, J. Effect of different heat treatments on the microstructure and mechanical properties in selective laser melted Inconel 718 alloy. *Mater. Manuf. Process.* **2017**, *32*, 1588–1595. [CrossRef]
32. Aydinöz, M.E.; Brenne, F.; Schaper, M.; Schaak, C.; Tillmann, W.; Nellesen, J.; Niendorf, T. On the microstructural and mechanical properties of post-treated additively manufactured Inconel 718 superalloy under quasi-static and cyclic loading. *Mater. Sci. Eng. A* **2016**, *669*, 246–258. [CrossRef]
33. Huang, L.; Cao, Y.; Li, G.; Wang, Y. Microstructure characteristics and mechanical behaviour of a selective laser melted Inconel 718 alloy. *J. Mater. Res. Technol.* **2020**, *9*, 2440–2454. [CrossRef]